Humidification of Air by Pressure Swirl Water Atomizer

M. G. Mousa

Mechanical Power Eng. Dept., Faculty of Engineering, Damietta University., New Damietta, Egypt.
Email: Mgmousa@mans.edu.eg

Abstract

In this paper, theoretical and experimental investigations are carried out to analyze the humidification process of air flowing horizontally over sprayed water from a pressure swirl nozzle inside a wind tunnel. A numerical model simulating the conservation of mass, momentum and energy of both water and air was developed to predict heat and mass transfer during process. Experimental investigation was performed, taking into account the impact of various parameters on the atomizer performance. The obtained data are used to validate the suggested model. Predictions of outlet air conditions for various air and water inlet conditions agreed well with the present experimental results and those in literature. On the basis of the model, the effects of inlet water and inlet air conditions on air outlet conditions are also analyzed.

Key words: Humidification of air; Heat and mass transfer; atomizers.

1. Introduction

Air humidification is the process in which water vapor content in air is increased. This process may be done by direct contact between co-flowing liquid water and air where, a portion of water vapor is transferred to the flowing air under the influence of water vapor concentration difference. In order to enhance the rate of water evaporation, surface area of contact between water and air should be increased. This can be achieved through an atomization process, which means the transformation of bulk liquid to droplets. Sirignano and Mehring [1] reviewed theory of distortion and disintegration of liquid streams. Lefebvre [2] described in detail different types of atomizers

Because of its wide range of applications, the pressure swirl atomizer has attracted the attention of many research works and has been the subject of considerable theoretical and experimental studies. Lefebvre [3] proposed an equation for the mean drop size produced by pressure-swirl atomizers. Nonnenmacher and Piesche [4] presented a theoretical model for predicting the Sauter mean diameter as a function of individual parameters of operation and material for pressure swirl atomizer, the results showed agreement with experimental data. Due to the random nature of atomization process, the resultant spray is usually characterized by a wide range of drop sizes and velocity magnitudes. Babinsky and Sojka [5] reviewed three available methods for modeling drop size distributions: the maximum entropy principal (MEP) method, the discrete probability function method, and the empirical method. The maximum entropy method is based on the use of the maximum entropy principle developed by Janes [6] from Shannon's [7] concept of entropy. This principle states that the most appropriate probability distribution is the one which maximizes Shannon's entropy subject to the given constraints imposed upon a physical system or process. For atomization, the most probable droplet size and velocity distribution can be obtained by maximizing Shannon's entropy under the constraints of the partial information known about the atomization process, i.e. the conservation laws

Semião et al. [8], used MEP method to develop a mathematical model for predicting drop size distribution of sprays which depends solely on Sauter mean diameter. Their results agreed well with their experimental data. Ayres et al. [9], extended the work of Semião et al. [8], to develop a mathematical model which is capable of predicting a joint distribution for size and

velocity of the spray droplets dependent on Sauter mean diameter and its average velocity. They used the joint distribution to obtain individual distributions for both the size and velocity of the spray droplets. They also developed a correlation for the average velocity of pressure swirl atomizer droplets, which fairly agreed their experimental data.

Nomenclature			
A	cross-section area of the test section	Sc	Schmidt number
A_s	surface area of drop	Sh	Sherwood number
A_p	area of ports of pressure-swirl atomizer	SMD	Sauter mean diameter
A_0	orifice area	T	temperature
C_D	droplet drag coefficient	t	liquid sheet thickness
C_{Dis}	coefficient of discharge	U	droplet velocity
C	specific heat of fluid	$\overline{U}$	liquid sheet mean velocity
c	water vapor concentration in air	u	air velocity
c_s	water vapor concentration in air at droplet surface	W	relative velocity of droplet with respect to air
D	diameter	x,y	coordinate directions
DBT	dry bulb temperature		

Greek symbols

d_0	orifice diameter	Γ	statistical gamma function
g	gravitational acceleration	μ	dynamic viscosity of the fluid
H	enthalpy	ρ	density of fluid
HTP	heat transfer potential	σ	surface tension
h	heat transfer coefficient	ω	air humidity ratio
h_{fg}	enthalpy of vaporization of water	θ	spray half cone angle
h_m	mass transfer coefficient	λ	diffusivity of water vapor in air
k_a	thermal conductivity of air		

Subscripts

MTP	mass transfer potential	a	air
M	momentum	i	droplet class
N	total number of droplets	in	inlet condition
$\dot{N}$	total number of droplets per unit time	j	integer index
$\dot{n}_i$	total number of droplets per unit time in droplet s	l	liquid
Nu	Nusselt number	out	outlet condition
Re	Reynolds number	s	surface
P	droplets probability	v	vapor
Pr	Prandtl number	x	x-direction
Δp_l	Pressure difference across atomizer	y	y-direction

Superscripts

Q_l	volume flow rate	m	number of droplets classes
		*	normalized variable

The two phase flow situation which arises when dispersed liquid phase co-flow with continues gas phase can be modeled through applying mass, momentum and energy conservation principles to each phase. The terms representing exchanges of mass, momentum, and energy between the two phases appear as source and sink terms in both the gas phase and the liquid phase equations. They provide the mathematical coupling between the two

subsystems of equations. Continuous gas phase conservation equations are described by Eulerian formulation while dispersed liquid phase equations are described either by Lagrangian or Eulerian formulation. If all droplets of the spray have the same inflow boundary conditions, the spray is called monodisperse spray and can be modeled by two system of governing equations, one for the liquid phase, and the other for gas phase. While the spray of different inflow boundary conditions is called polydisperse spray. In such case, every set of droplets of the same inflow boundary condition forms droplet class and the two phase flow situation can be modeled by a system of equations describing gas phase and multi-system of equations describing each droplet class. The resulting governing conservation equations of the two phases can then be solved simultaneously. Ahmed Dar and Bannikov [10] studied the design of a swirl atomizer which provides a certain flow rate of water with required spray quality for effective evaporative cooling of high temperature compressed air The evaporative cooling decreases the intake air temperature of engine and increases its mass flow rate, with constant fuel-to-air ratio this increase in air mass flow rate increases the power of the engine. The atomizer was tested experimentally and through fluid flow modeling for its required spray quality and the results were fairly close with theoretically predicted results. The design of atomizer was also optimized for required spray characteristics by modeling the fluid flow inside the atomizer. Sharma et al [11] a detailed and discussion on its design, and operation. Experiments are performed on seven atomizers to study the effect of design, and operating parameters on spray cone angle, and average droplet diameter. Spray cone angle remains constant with change in air mass flux, and increases with increasing orifce diameter, and manifold diameter. Nearcomplete suppression of atomizer clogging makes our new additively-manufactured perforated plate atomizer an ideal ft for high salinity, and zero liquid discharge humidifcation-dehumidifcation desalination systems. Additionally, its open-surface design allows additional surface modifcations to further reduce clogging, and enhance self-cleaning characteristics

The aim of the present study is to develop a theoretical model for predicting air humidification process by a pressure swirl atomizer. The effects of inlet conditions for both sprayed water and air on the leaving air conditions are considered. Test rig is built to carry out experiments for the sake model validation. The theoretical study also involved the predictions of the effect of inlet water and air conditions on the humidification process using such water atomizing devices.

2. Theoretical Model

In order to develop a theoretical model for predicting the flow field of air and water droplets in humidification process, two phase flow model is employed; one for describing water-air flow field, and the other for water atomization process to describe the droplet size and velocity distribution at the inlet of the flow field domain.

2.1 Two Phase Flow Model:

2.1.1 Mechanism and Assumptions

Steady water spray originating from atomizer in two dimensional system forms with a uniform steady one dimensional laminar air flow a two phase flow situation with isolated boundaries, as illustrated in Fig.1. This situation can be modeled through applying conservation principles for the two phases. The interactions between droplets, change in air momentum, heat and mass diffusion through air, and the effect of liquid film over the duct wall on heat and mass transfer to air, are assumed to be neglected.
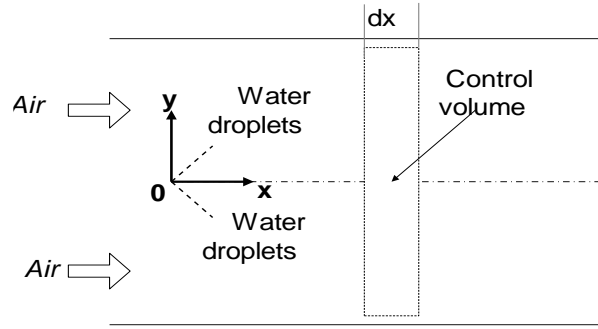
Fig. 1 System for flow modeling

2.1.2 The Governing equations

Mass conservation yields an equation expressing the change in droplet diameter, given by

$$\frac{dD_i}{dx} = -\frac{2h_{m,i}\rho_a A_{s,i}(c_{s,i} - c)}{\rho_l U_{x,i}} \qquad (1)$$

Momentum conservation yields equations expressing the change in droplet velocity, described as:

$$\frac{dU_{x,i}}{dx} = -\frac{3C_{D,i}\rho_a W_i(U_{x,i} - u)}{4D_i\rho_l U_{x,i}} - \frac{3U_{x,i}}{D_i}\frac{dD_i}{dx} \qquad (2),$$

and

$$\frac{dU_{y,i}}{dx} = -\frac{g(\rho_l - \rho_a)}{U_{x,i}\rho_l} - \frac{3C_{D,i}\rho_a W_i U_{y,i}}{4D_i\rho_l U_{x,i}} - \frac{3U_{y,i}}{D_i}\frac{dD_i}{dx} \qquad (3)$$

The droplets trajectories is given by

$$\frac{dy_i}{dx} = \frac{U_{y,i}}{U_{x,i}} \qquad (4)$$

Energy conservation yields equations expressing the change in droplet temperature, expressed as:

$$\frac{dT_i}{dx} = \frac{6\left[h_i(T_a - T_i) - h_{fg,i}h_{m,i}\rho_a(c_{s,i} - c)\right]}{D_i\rho_l U_{x,i}C_{p,l}} - \frac{3T_i}{D_i}\frac{dD_i}{dx} \qquad (5)$$

Conservation of water vapor mass yields equation describing the change in concentration, given by

$$\frac{dc}{dx} = \frac{1}{uA}\sum_{i=1}^{m}\frac{\dot{n}_i h_{m,i}A_{s,i}(c_{s,i} - c)}{U_{x,i}} \qquad (6),$$

and the conservation of energy yields equation expressing the change of air temperature, described as

$$\frac{dT_a}{dx} = \frac{1}{uA\rho_a C_{p,a}}\sum_{i=1}^{m}\frac{\dot{n}_i A_{s,i}}{U_{x,i}}\left[h_{fg,i}h_{m,i}\rho_a(c_{s,i} - c) - h_i(T_a - T_i)\right] - \frac{h_v}{C_{p,a}}\frac{dc}{dx} \qquad (7)$$

2.1.3 Boundary conditions:

The above governing equations are ordinary differential equations of first order so; they need inflow boundary conditions only which are defined for the variables, follow as:

$$D_i(0) = D_{i,in}, \; U_{x,i}(0) = U_{x,i,in}, \; U_{y,i}(0) = U_{y,i,in} \quad, y_i(0) = 0.0, \; T_i(0) = T_{l,in} \qquad (8)$$

2.2 Spray characterization

The model developed by Ayres et al [9] is used to describe droplet size and velocity distributions of the spray. Droplet size distribution is given by:

$$P(D) = \int_{D_j}^{D_{j+1}} 3\Gamma\left(\frac{5}{3}\right)^{-3} \left(\frac{D}{SMD}\right)^2 \times \exp\left[-\Gamma\left(\frac{5}{3}\right)^{-3}\left(\frac{D}{SMD}\right)^3\right] \frac{dD}{SMD} \qquad (9)$$

Droplet velocity distribution is given by:

$$P(U) = \int_{U_j}^{U_{j+1}} \Gamma\left(\frac{3}{2}\right)^{-4} \left(\frac{U}{\overline{U}}\right) \times \left[1 + \frac{1}{2}\Gamma\left(\frac{3}{2}\right)^{-4}\left(\frac{U}{\overline{U}}\right)^2\right]^{-2} \frac{dU}{\overline{U}} \qquad (10)$$

Joint size/velocity distribution is given by:

$$P(D,U) = \int_{D_j}^{D_{j+1}} \int_{U_j}^{U_{j+1}} 3\Gamma\left(\frac{3}{2}\right)^{-4}\Gamma\left(\frac{5}{3}\right)^{-6}\left(\frac{U}{\overline{U}}\right)\left(\frac{D}{SMD}\right)^5 \times \exp\left[-\Gamma\left(\frac{5}{3}\right)^{-3}\left(\frac{D}{SMD}\right)^3\right.$$
$$\left. -\frac{1}{2}\Gamma\left(\frac{5}{3}\right)^{-3}\Gamma\left(\frac{3}{2}\right)^{-4}\left(\frac{U}{\overline{U}}\right)^2\left(\frac{D}{SMD}\right)^3\right] \frac{dD}{SMD} \frac{dU}{\overline{U}} \qquad (11)$$

Here, $\overline{U}$ is the liquid sheet mean velocity given by [9] as:

$$\overline{U} = \frac{320}{147}\frac{Q_l}{\pi d_0^{\,2}} \qquad (12)$$

The number of droplets in each droplet class is given by

$$\dot{n}_i = \dot{N} \times P_i(D,U) \qquad (13)$$

The total number of droplets is then given by

$$\dot{N} = \frac{Q_l}{\left(\pi/6\right)SMD^3}\Gamma\left(\frac{5}{3}\right)^{-3} \qquad (14)$$

A normalized droplets total surface area is described as

$$A_s^* = \frac{\sum\limits_{i=1}^{m} n_i D_i^2}{\sum\limits_{i=1}^{m} n_i D_i^2 (0)}$$
(15)

2.3 The Used correlations

In the analysis, several correlations are used and described as follows:

2.3.1 Drag coefficient

The droplet drag coefficient suggested by [16] is given by

$$C_{D,i} = \frac{24(1 + 0.15\text{Re}_i^{0.687})}{\text{Re}_i}, \text{ for } 0 < \text{Re}_i < 1000$$
(16)

And for $1000 < \text{Re}_i$ the value of $C_{D,i} = 0.44$

Here, Re_i is the droplet Reynolds number based on the velocity of droplets relative to the air, given by:

$$\text{Re}_i = \frac{\rho_a W_i D_i}{\mu_a}$$
(17)

Where

$$W_i = \sqrt{[U_{x,i} - u]^2 + U_{y,i}^2}$$
(18)

2.3.2 Mass concentration properties

The mass concentration of water vapor at droplet surface is given by:

$$c_s = \frac{0.622 P_{v,s}}{P_a + 0.622 P_{v,s}}$$
(19)

Where P_a is barometric pressure of dry air, and $P_{v,s}$ is the saturation pressure of water vapor corresponding to the air temperature, T, given by:

$$P_{v,s} = \exp[-5800.2206/T + 1.3914993 - 0.048640239T + 0.41764768 \times 10^{-4}T^2$$

$$- 0.14452093 \times 10^{-7}T^3 + 6.5459673\log T]$$
(20)

The humidity ratio can be expressed as:

$$\omega = \frac{c}{1-c} \tag{21}$$

2.3.3 Heat and mass transfer correlations

the correlations for heat and mass transfer coefficients as reported by [17] given by

$$Nu_i = \frac{h_i D_i}{k_a} = 2 + 0.6 \mathrm{Re}_i^{0.5} \mathrm{Pr}^{0.33} \tag{22}$$

$$Sh_i = \frac{h_{m,i} D_i}{\lambda} = 2 + 0.6 \mathrm{Re}_i^{0.5} Sc^{0.33} \tag{23}$$

Where Sc, and Pr are Schmidt number and Prandtl number, respectively, defined as

$$Sc = \frac{\mu_a}{\rho_a \lambda} \tag{24-a},$$

$$\mathrm{Pr} = C_{p,a} \frac{\mu_a}{k_a} \tag{24-b}$$

The mass diffusivity of water vapor in air, λ has been estimated from the relation developed by Bird et al. [18], given by

$$\lambda = 2.495 \times 10^{-5} \left(\frac{T_a}{292.88} \right)^{2.334} \tag{25}$$

2.3.4 Sauter Mean Diameter of Spray

Sauter mean diameter of spray is the ratio of the total volume of the spray to its total surface area and is correlated by Lefebvre [3] as:

$$SMD = 4.52 \left(\frac{\sigma \mu_l^2}{\rho_a \Delta p_l^2} \right)^{0.25} (t \cos\theta)^{0.25}$$

$$+ 0.39 \left(\frac{\sigma \rho_l}{\rho_a \Delta p_l} \right)^{0.25} (t \cos\theta)^{0.75} \tag{26}$$

Where t is the liquid sheet thickness given by [19]:

$$t = 2.7 \left[\frac{d_0 FN \mu_l}{(\Delta p_l \rho_l)^{0.5}} \right]^{0.25} \tag{27},$$

The liquid flow number, FN is given by:

$$FN = \frac{Q_l \rho_l}{\sqrt{\Delta p_l \rho_l}} \tag{28},$$

and ΔP is the liquid pressure difference across the atomizer, given by::

$$\Delta p_l = \frac{Q_l^2 \rho_l}{2 C_{Dis}^2 A_0^2}$$ (29)

The atomizer discharge coefficient, C_{Dis} is assumed to be equal to 0.25

The spray half cone angle is given by [20]

$$\theta = 3 \left(\frac{A_p}{D_{sw} d_0} \right)^{-0.15} \left(\frac{\Delta p_l d_0^2 \rho_l}{\mu_l^2} \right)^{0.11}$$ (30)

2.4 Heat and mass transfer potentials

In cocurrent flow heat exchangers, the potential for heat transfer is the inlet temperature difference between the two fluids. However, in evaporative cooling situation, there is a direct contact between water and air. So, the temperature difference between air and water doesn't describe the potential for heat transfer. Another parameter should be used to describe this potential, named as the heat transfer potential described as:

$$HTP = h_{fg,in} \rho_a \left(\frac{\lambda_{in}}{k_a} \right) (c_{s,in} - c_{in}) - (T_{a,in} - T_{l,in})$$ (31)

Similarly, the mass transfer potential is expredssed:

$$MTP = (c_{s,in} - c_{in})$$ (32)

2.5 Numerical solution procedure

The governing equations describing the two phase flow problem under consideration are first order ordinary differential equations. The solution of theses equations need inflow boundary conditions only. Upstream conditions of air dry bulb temperature and water vapor concentration are prescribed. For liquid phase, the droplet sizes and velocities whose probability less than prescribed values are omitted by solving Eq 27 and Eq. 28. They provide boundaries for the computational domain of droplet classes. This domain is discredited to five droplet diameters and ten droplet velocity magnitudes in two directions, resulting in 100 droplet classes. Number of droplets in each class is computed using Eq. 29 and Eq. 30. Droplet classes are assumed to have the same temperature as the upstream air temperature.

A FORTRAN code is developed to solve the governing equations for the two phases numerically for a given duct dimensions using Euler method. The conditions at various downstream locations are then computed. When the diameter of a droplet class vanishes or the droplet class hits the wall of the duct; this droplet class is excluded from computation.

3. Experimental setup

A schematic diagram of the experimental facility is shown in Fig. 2. Ambient air is sucked by a variable speed axial fan (6) driven by variable speed electric motor (7) into the flow conditioning section (1). Air enters the test section (2) of dimensions $0.3 \times 0.3 \times 2$ m, and interacts with water spray emerging from atomizer (13). At the end of the test section a mist

eliminator (3) is placed to prevent water droplets from entering to the outlet air measuring section (4). Water is pumped from a tank (9) by a centrifugal pump (10). Drainage is collected at the end of test section through collecting tank (14).

Air velocity is measured by a vane probe at different locations in the duct section (4) when the axial fan is turned on, then the pump is turned on and water spray enters the test section and interacts with the air. After the system reaches to the steady state, inlet air temperature and humidity ratio are measured upstream of the atomizer by a hygrometer, and the water flow rate is measured by a flow meter (12). Water inlet temperature is measured by a thermocouple impeded in the pipe connecting atomizer with flow meter (12). Air outlet temperature and humidity ratio are measured by the hygrometer at duct section (4).

1. Flow conditioning section   8. Control valve
2. Test section   9. Water tank
3. Mist eliminator   10. Water pump
4..Outlet air measuring section   11. Control valve
5. Diffuser   12. Water flow meter
6. Axial fan   13. Atomizer
7. Electric motor   14. Collecting tank
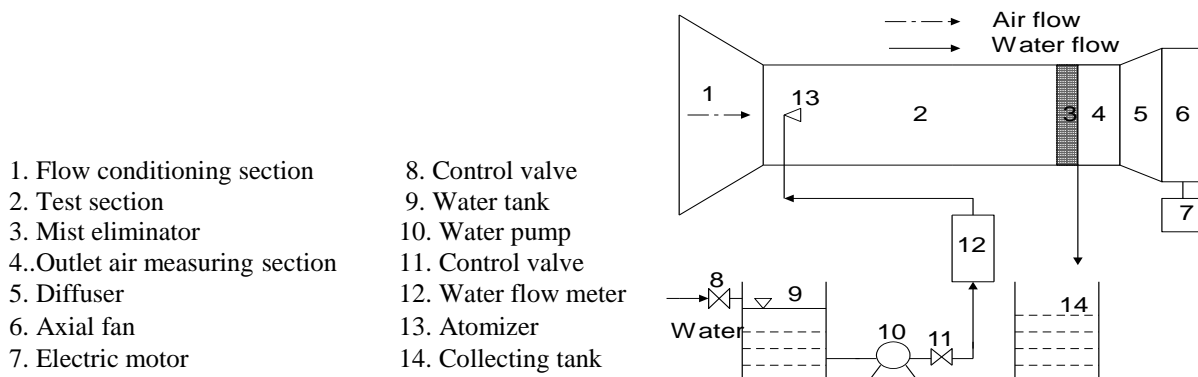
Fig. 2 Schematic diagram of wind tunnel facility

4. Results and discussion

4.1. Investigation of model validity

Table 1 shows the different working conditions in which experiments and calculations were carried out.

Table 1: Working conditions for experimental and calculation

Condition	Water inlet conditions		Air inlet conditions		
	$Q \times 10^6$ (m³/s)	T (ºC)	u (m/s)	DBT (ºC)	$c \times 10^3$ (kg/kg)
1	7.71	20.0	1.65	22.7	12.83
2	17.33	20.0	2.075	22.9	12.6
3	17.237	20.0	2.5	23.1	13.4
4	18.17	24.0	1.498	25.3	14.778
5	18.17	24.0	2.5	25.4	15.6
6	27.9	24.5	2.075	26.2	15.166
7	20.964	24.7	2.5	26.3	15.748
8	22.362	19.0	1.92	19.8	10.0

Comparisons between measured and calculated dry bulb temperature and water vapor concentration are shown Figs. 3 and 4, respectively. It can be observed from Fig. 3 that the theoretical model predictions have higher values of dry bulb temperature (DBT) than those

measured, because the model does not take into account the effect of liquid film which flows over the lower duct surface and also the effect of mist eliminator. This film has lower temperature than that of the flowing air which results in lowering the measured DBT than those predicted. For water vapor concentration, the model predictions are very close to those measured and the effects of water film and mist eliminator don't appear because air is almost saturated with water vapor at exist.
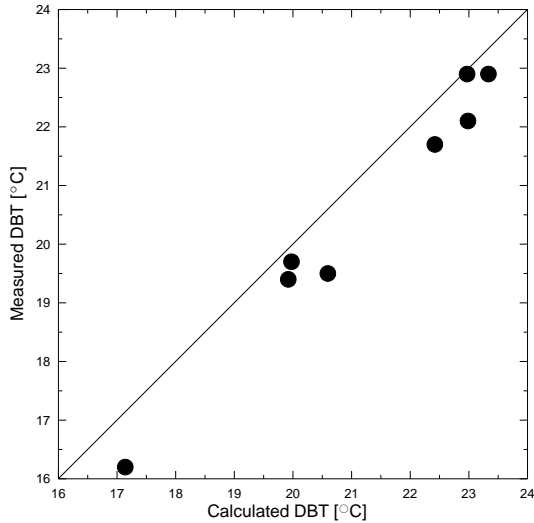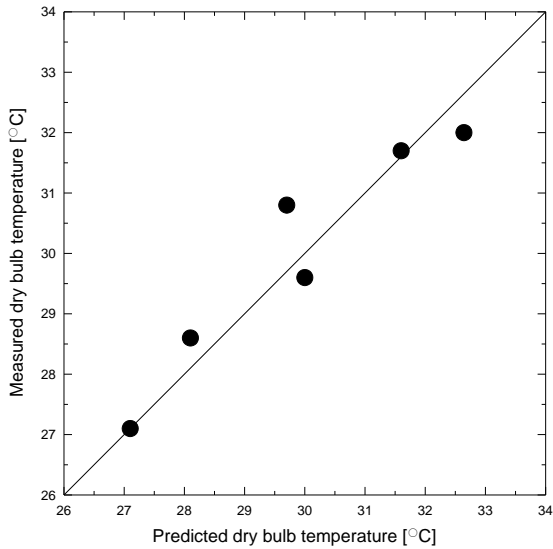

Fig. 3 Comparison between measured and calculated DBT
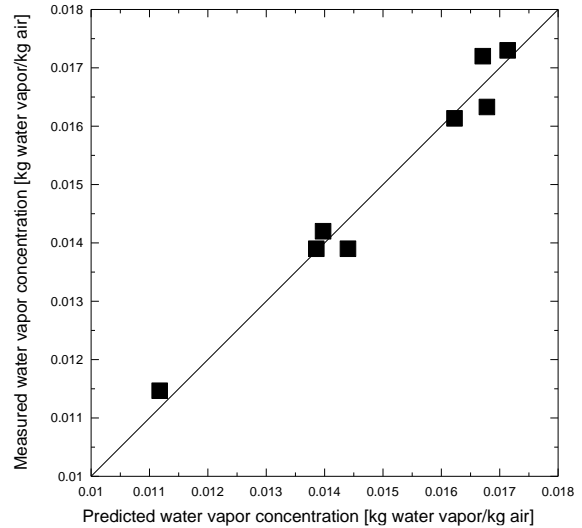
Fig. 4 Comparison between measured and calculated water vapor concentration

Profiles of dry bulb temperature, water vapor concentration, normalized droplets surface area along duct length for condition 1, are shown in Figs. 5 to 7.
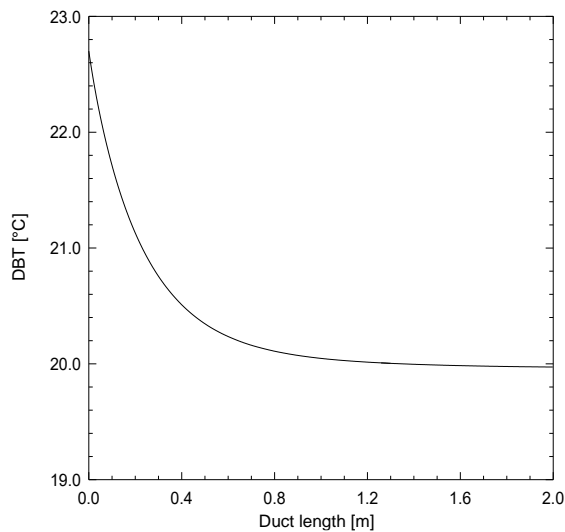
Fig. 5 Predicted DBT along duct
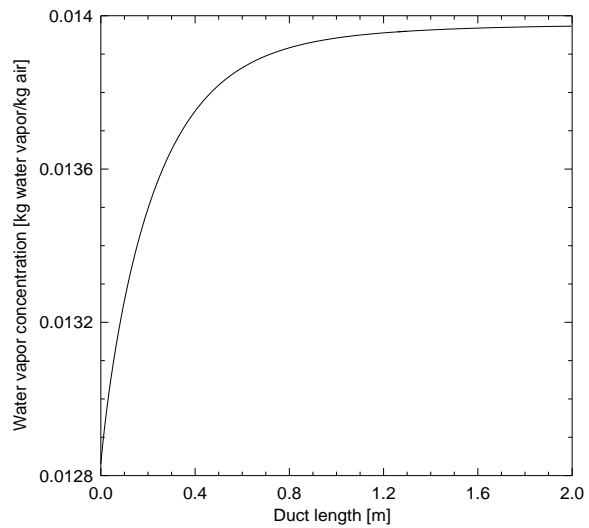
Fig. 6 Predicted water vapor concentration along duct length
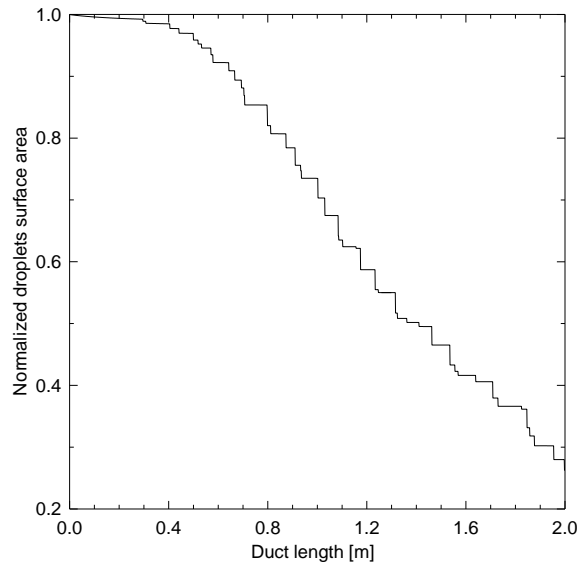
Fig. 7 Normalized droplets surface area along duct length

Table 2 shows the operating conditions of Sureshkumar et al [17] where, water flow rate of 18.33 l/min, pressure difference across atomizer of 3 bar, spray half cone angle 39° of and *SMD* of 227µm were considered.

Comparison between experimental results of Sureshkumar et al [17] and the present calculated dry bulb temperature and water vapor concentration are shown in Figs. 8 and 9, respectively. As can be shown in Fig. 8, the values of measured DBT [17] are normally distributed around the line of equal measured and predicted ones. In Fig. 9, However, . the first three values of measured water vapor concentration are relatively far from the predicted values. This is because that the working conditions for these have low inlet humidity ratio and high heat transfer potential which resulted in a relatively big difference between measured and predicted water vapor concentration. Another reason for this discrepancy is due to the uncertainty in measured values of Sauter mean diameter, *SMD*.

Table 2: Working conditions for experimental [14] and calculation

Cond	Water inlet	Air inlet		
	T (°C)	u (m/s)	DBT (°C)	c×10³(kg/kg)
1	32.0	1.0	40.1	16.716
2	33.3	2.0	39.6	16,716
3	33.4	3.0	38.9	16.522
4	35.8	1.0	41.4	4.98
5	35.0	2.0	40.0	4.58
6	35.5	3.0	38.7	6.557

Fig. 8 Comparison between measured data[17] and calculated DBT.
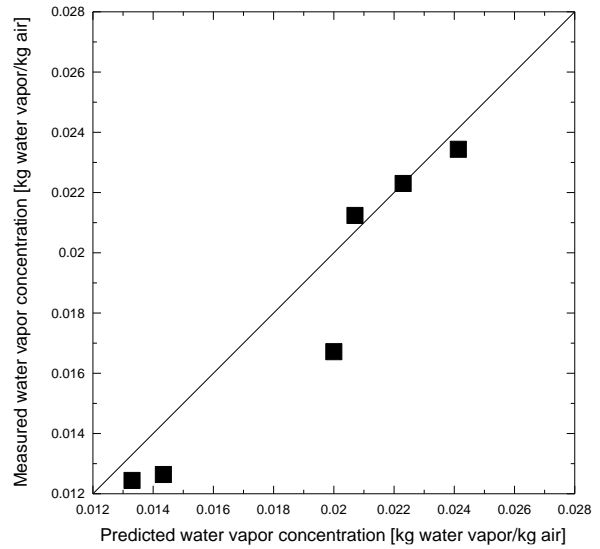
Fig. 9 Comparison between measured [17] and calculated water vapor concentration

Figures 10 and 11 show the effect of *SMD* uncertainty on exit dry bulb temperature and water vapor concentration of flowing air for condition 4 in Ttable: 2
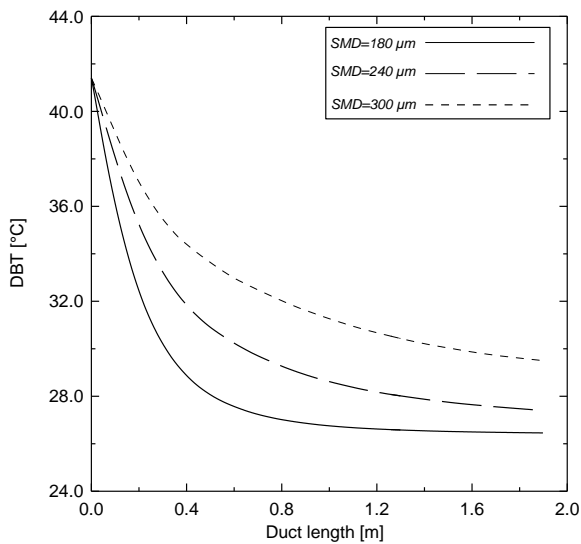

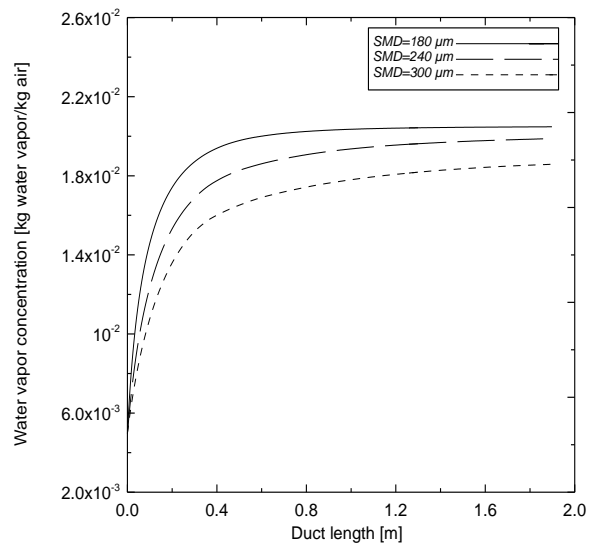Fig. 10 Predicted dry bulb temperature along duct length at different *SMD*

Fig.11. Predicted water vapor concentration along duct length, at different SMD

4.2.1 Heat and mass transfer potentials

Figure 12 shows the dry bulb temperature depression with heat transfer potential, HTP. It can be observed that the change in DBT tremendously increases with increasing HTP. Consequently, the effectiveness of heat transfer $((DBT_{in} - DBT_{out})/HTP)$ decreases with increasing *HTP*, as can be seen in Fig.13.
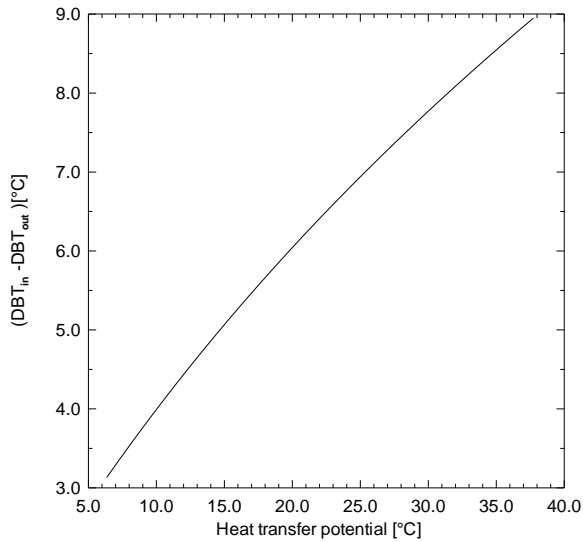
Fig. 12. Predicted DBT change with heat transfer potential, HTP
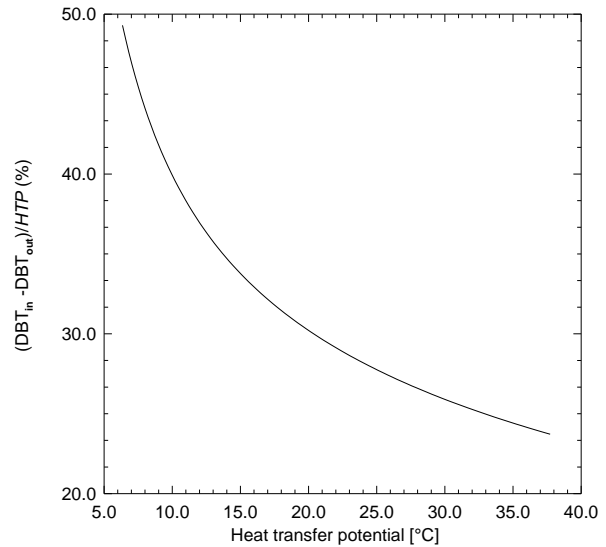
Fig. 13 Variation of heat transfer effectiveness with heat transfer potential, HTP

Figure 14 shows the change in water vapor concentration in the flowing air with mass transfer potential, *MTP*. As expected, the rate of evaporation is highly increased with increasing *MTP*, leading to a great change in water vapor concentration. This resulted in a tremendous reduction in the effectiveness of mass transfer ($(c_{out} - c_{in})/MTP$) with increasing *MTP*, as shown in Fig. 15 (These predicted results are related to an operating conditions: air velocity of 1.65 m/s and water flow rate of 17.7×10^{-6} m³/s).
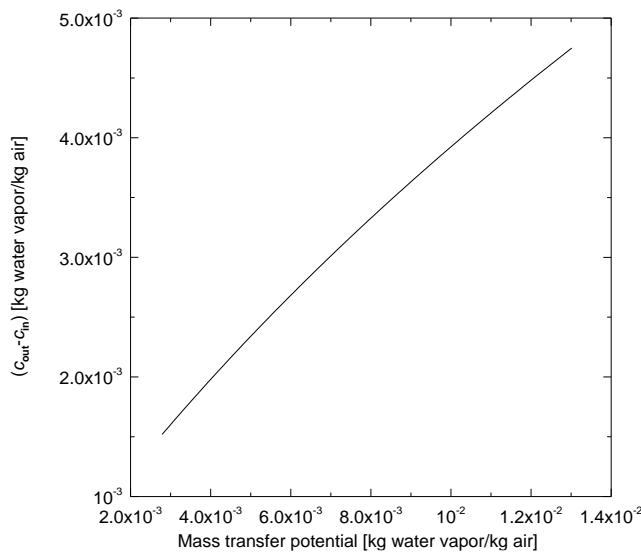
Fig. 14. Predicted water vapor concentration change with mass transfer potential, MTP
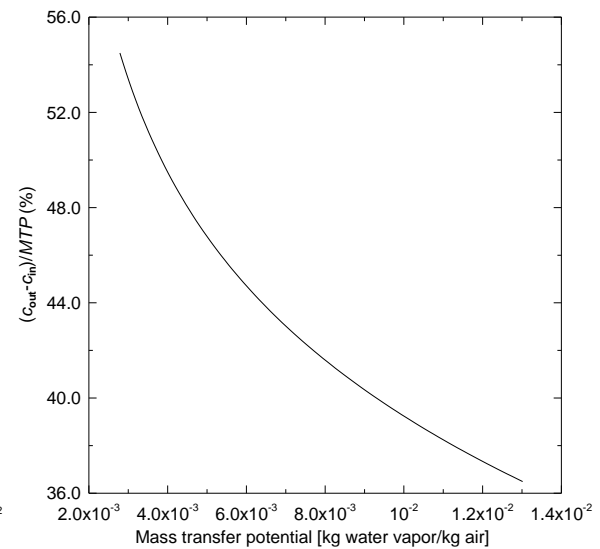
Fig. 15. Variation of mass transfer effectiveness with MPT

4.2.2 Effect of air flow rate

Figure16 shows the variation of water vapor concentration change with air velocity at different values of mass transfer potential. At a certain MTP, the increase in water vapor concentration decreases with increasing air velocity. At the same time, as MTP gets higher value, the change in water vapor concentration becomes higher. The rate of vaporized water is greatly affected by both air velocity and MTP. As can be noticed in Fig. 17, the vaporized

water mass rate tremendously increased with increasing air velocity. As MTP gets higher value, the rate of evaporation becomes higher.
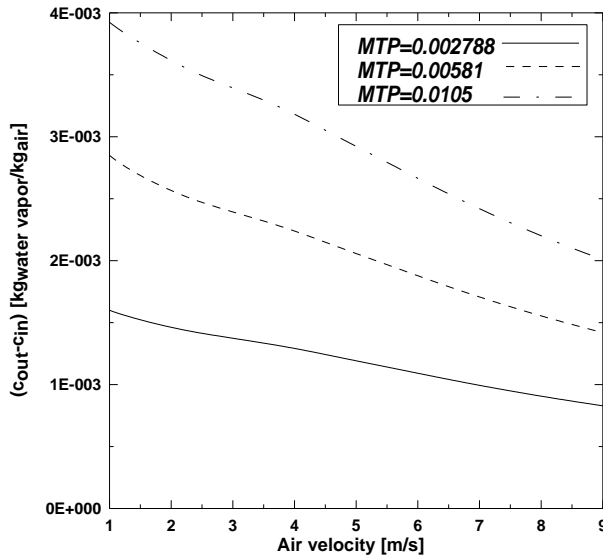

Fig. 16 Water vapor concentration change versus air velocity at different values of MPT
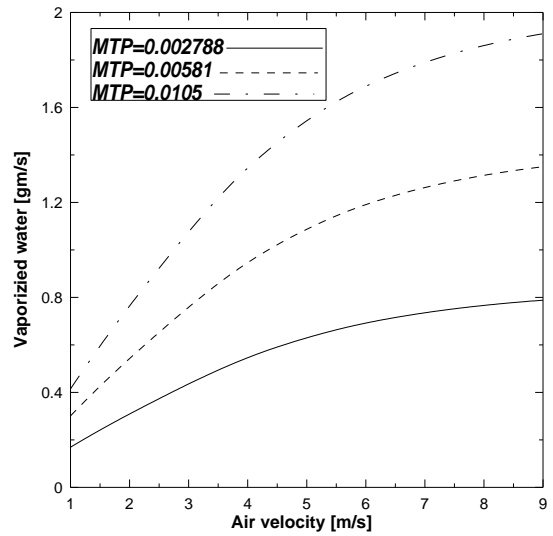
Fig.17 Rate of vaporized water versus air velocity at different values of MPT

Figure18 shows the effect air flow rate on DBT change at different values of HTP (Duct dimensions are those of experimental, and water flow rate of $17{\times}10^{-6}$ m³/s). It can be observed that the change in DBT generally decreases with increasing air flow rate. In the mean time, as the mass transfer potential increases, the change in DBT becomes higher.
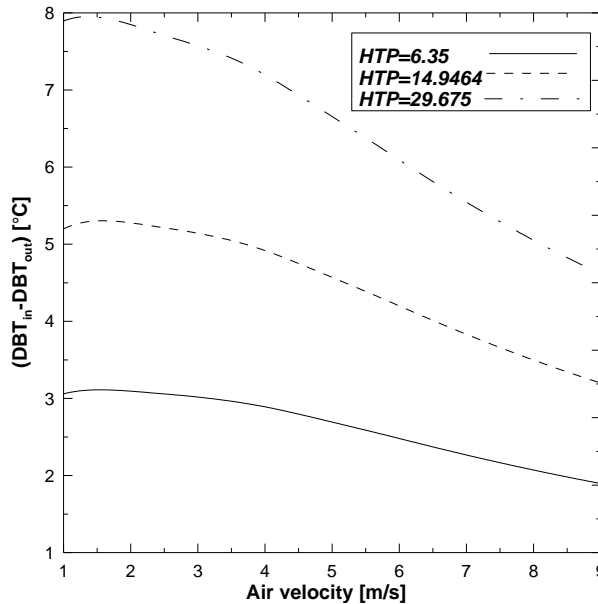

Fig. 18 DBT depression versus air velocity at different values
of heat transfer potential,

4.2.3 Effect of water flow rate

Figure 19 shows the effect of mass flow rate of sprayed water on the changes in DBT at different values of HTP. It can be observed that the variation in mass rate of water has a relatively small effect on DBT changes. Meanwhile, as the HTP increases, the change in DBT gets higher vales as discussed above. The same trends are also noticed for the change in water

vapor concentration with the variation of mass flow rate of sprayed water as can be noticed in Fig. 20 (Duct dimensions are those of experimental, air velocity is 2 m/s)
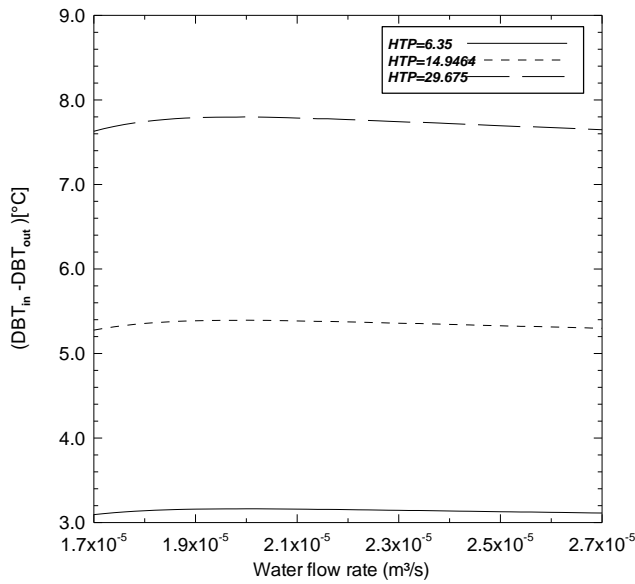

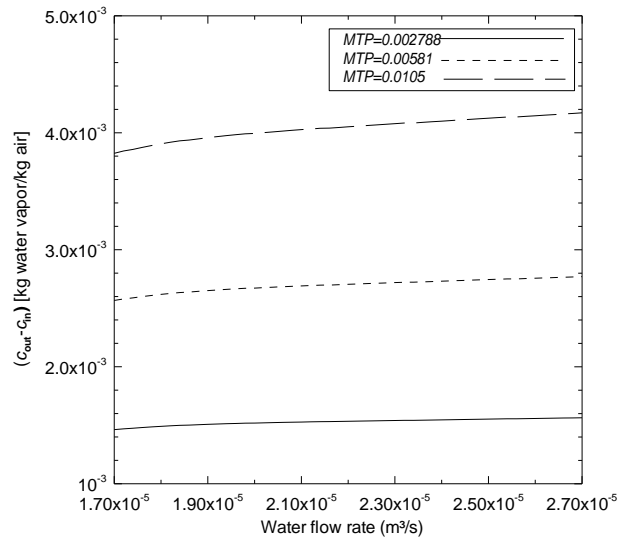Fig. 19 DBT change with water flow rate at different values of HTP

Fig. 20 Water vapor concentration change with water flow rate at different values of MTP

4.2.4 Effect of duct width

In order to study the effect of changing duct width on the humidification process, the duct width is varied from 0.2m to 1.2m, while keeping a constant air velocity of 2m/s, a constant duct length of 2mm, and water flow rate of 17×10^{-6} m³/s. Figure 21 shows DBT change with duct side length at different values of HPT. It can be noticed that the DBT depression generally decreases with increasing duct width. It is also observed that the variation of duct width has the same effect on the change in water vapor concentration among the flowing air. This can be shon in Fig. 22, where the change in water vapor concentration decreases with increasing the duct width at a certain value of MTP. However, the rate of vaporized water tremendously increased with increasing the duct width as can be noticed in Fig.23
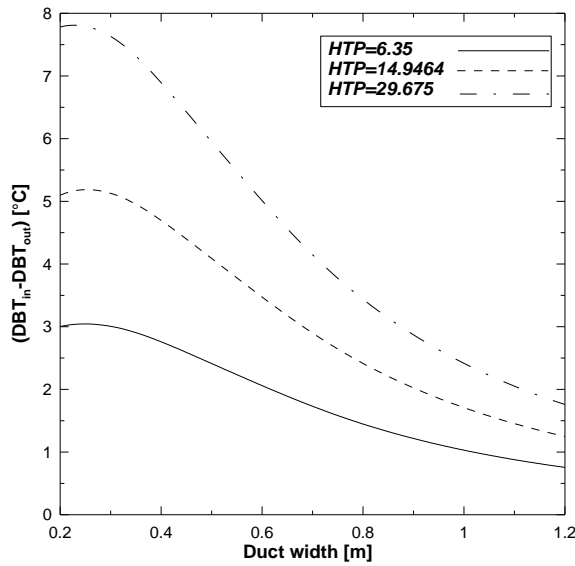
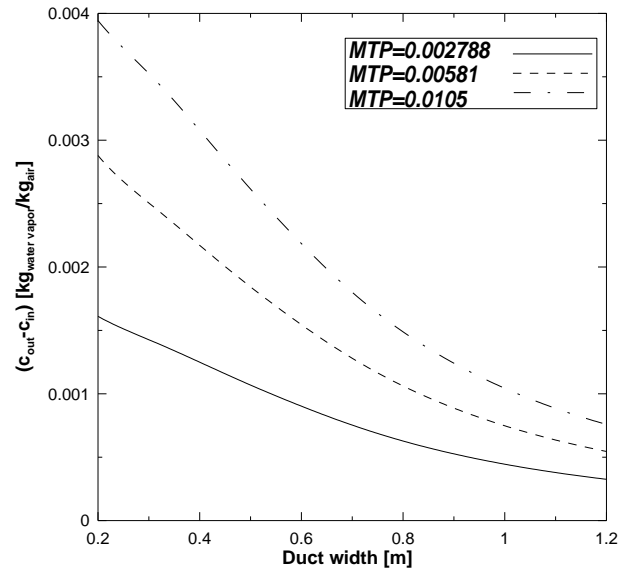Fig. 21. Predicted DBT change with duct width at different values of HTP

Fig. 22. Predicted water vapor concentration change Versus duct width at different values of MTP
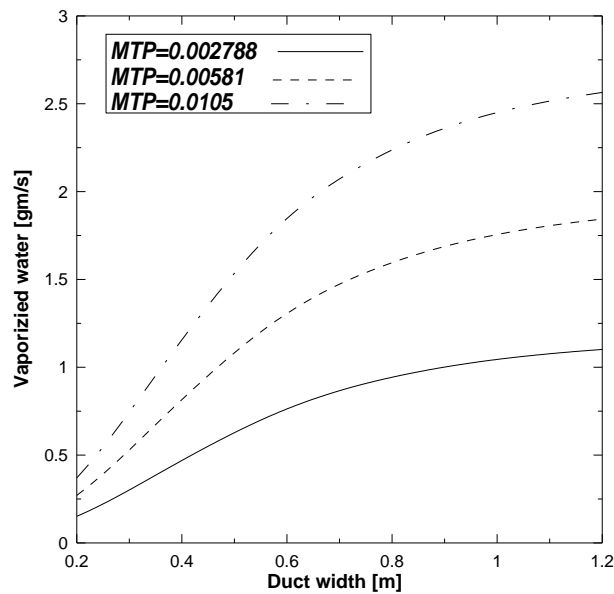

Fig. 23 Rate of vaporized water versus duct width at different values of MTP

(Air velocity = 2m/s, water flow rate1=7×10^{-6} m³/s)

5. Conclusions

In this study a numerical model for predicting heat and mass transfer between sprayed water from a pressurized swirl nozzle and air stream in horizontal parallel flow configuration was developed. The model inputs are inlet water temperature and its flow rate, inlet air dry bulb temperature and humidity ratio, atomizer geometry and duct dimensions. The inputs of droplet size/velocity distributions are not considered. The model predictions agreed well with experimental data taken and those in literature. The effects of various air and sprayed water parameters on humidification process are thoroughly investigated. The results showed that the droplets mean diameter has the most effect on heat and mass transfer predictions. Further

research on modeling of atomization process will improve the capability of existing models in predicting heat and mass transfer in such situations.

References

[1] W.A. Sirignano, C. Mehring, Review of theory of distortion and disintegration of liquid streams, Progress in Energy and Combustion Science 26 (2000) 609–655.

[2] A.H. Lefebvre, Atomization and Sprays, Hemisphere Publishing Corporation, New York, 1989.

[3] A. H., Lefebvre, The prediction of Sauter mean diameter for simplex pressure-swirl atomizers, Atomization Spray Technol. 3 (1987) 37-51.

[4] S. Nonnenmacher, M. Piesche, Design of hollow cone pressure swirl nozzles to atomize Newtonian fluids, Chemical Engineering Science 55 (2000) 4339-4348.

[5] E.Babinsky, P.E. Sojka, Modeling drop size distributions, Progress in Energy and Combustion Science 28 (2002) 303-329.

[6] E. T., Jaynes, Information theory and statistical mechanics, Physics Review 106 (1957) 620-630.

[7] C. E., Shannon, Bell System Technology Journal 27 (1948) 379-423.

[8] V. Semião, P. Andrade, M. da Graça Carvalho, Spray characterization: numerical prediction of Sauter mean diameter and droplet size distribution, Fuel 75(1996) 1707-17141.

[9] D. Ayres, M. Caldas, V. Semião , M. da Graça Carvalho, Prediction of the droplet size and velocity joint distribution for sprays, Fuel 80 (2001) 383-394.

[10] Uzair Ahmed Dar 1;2 and Mykola Bannikov Swirl Atomizer Design for Evaporative Cooling of High Temperature Compressed Air Stream International Journal of Fluid Mechanics Research, Vol. 41, No. 1, 2014

[11] Deepak Sharma, Durga Prasad Ghosh, Jordan Neal Rote, Sandra Jean Dennis, Morgan Messer, Xiang Zhang, Bahman Abbasi Development of an anti-clogging perforated plate atomizer for a zero liquid discharge humidifcation - dehumidifcation desalination system Desalination 515 (2021) 115195